

## Optically detected magnetic resonance of indirect excitons in an ensemble of (In,Al,Ga)As/(Al,Ga)As quantum dots

V. Yu. Ivanov <sup>1,\*</sup>, D. O. Tolmachev <sup>2</sup>, T. S. Shamirzaev <sup>3,4,†</sup>, T. Słupinski <sup>1</sup>, D. R. Yakovlev <sup>2,5</sup> and M. Bayer <sup>2,5</sup>

<sup>1</sup>*Institute of Physics, Polish Academy of Sciences, PL-02-668 Warsaw, Poland*

<sup>2</sup>*Experimentelle Physik 2, Technische Universität Dortmund, 44221 Dortmund, Germany*

<sup>3</sup>*Rzhanov Institute of Semiconductor Physics, Siberian Branch of the Russian Academy of Sciences, 630090 Novosibirsk, Russia*

<sup>4</sup>*Ural Federal University, 620002 Yekaterinburg, Russia*

<sup>5</sup>*Ioffe Institute, Russian Academy of Sciences, 194021 St. Petersburg, Russia*



(Received 9 August 2021; revised 14 September 2021; accepted 9 November 2021; published 18 November 2021)

The energy level structure as well as the exciton recombination and spin dynamics are studied in a dense ensemble of (In,Al,Ga)As/(Al,Ga)As quantum dots (QDs). The band alignment in the QDs is shown to have type-I, indirect character with the lowest electron state at the  $X$  valleys of the conduction band and the top hole state in the  $\Gamma$  point of the valence band, so that indirect excitons are formed in the QDs. Time-resolved photoluminescence and magnetic-field-induced circular polarization allow us to distinguish electron states belonging to the QDs and the wetting layer. Suppression of the exciton migration within the QD ensemble and along the wetting layer in the magnetic field is found. A pronounced effect of applied microwave radiation on the recombination and spin polarization of the indirect excitons is observed in longitudinal magnetic fields. Optically detected magnetic resonance (ODMR) is detected in both the intensity and the circular polarization degree of the QD emission. The ODMR resonance corresponds to the  $g$  factor of 1.97, associated with  $X$ -valley electrons. The spin relaxation time of the  $X$ -valley electrons is measured to be  $600 \pm 25$  ns.

DOI: [10.1103/PhysRevB.104.195306](https://doi.org/10.1103/PhysRevB.104.195306)

### I. INTRODUCTION

Structures with quantum dots (QDs) have been intensely studied for decades by now due to their potential for the fabrication of novel devices [1,2]. Among the large variety of QDs, those with indirect band gap have many advantages for spintronics devices. They demonstrate intense luminescence up to room temperature, provided by the strong localization of electrons and holes confined in the QDs by barriers with a large band gap [3]. The momentum separation of electrons and holes allows one to increase the exciton lifetime in such QDs up to hundreds of microseconds in heterostructures of type I [4], and an additional increase of the lifetime is achieved by spatial separation of the charge carriers in indirect band-gap heterostructures of type II [5]. These long exciton lifetimes make the latter structures highly interesting for studying the exciton spin dynamics and, in particular, seeking for long electron spin relaxation times which, according to theoretical estimations, may reach milliseconds [6]. The weak exchange interaction for the electron in the  $X$  valley of the conduction band with the  $\Gamma$  hole [7] results in a very small fine structure splitting of the excitons that make such QDs a prospective source of entangled photon pairs [8]. Also, the weak electron-nuclei interaction in the  $X$  valley makes the electrons robust against spin decoherence [9]. These features of the exchange and hyperfine interactions provide a

specific mechanism of spin polarization: dynamic electron spin polarization can take place in indirect band gap QDs for unpolarized optical excitation in weak magnetic fields of the order of a few millitesla [10].

Optically detected magnetic resonance (ODMR) is a powerful technique that has been successfully applied to study the spin levels and spin dynamics of bulk semiconductors and their low-dimensional structures [11–13]. In this technique the spin states of charge carriers or exciton complexes are addressed by microwave radiation in which photon energy is resonant with their Zeeman splitting. The induced changes are detected optically via the emission intensity and/or the polarization degree of the emission in the vicinity of the band gap. Spectral selectivity allows one to distinguish the various origins of ODMR signals [14,15]. A limitation of the ODMR technique is that the optical recombination rate should be comparable to or less than the microwave-induced transition rate between the exchange and/or magnetic-field-split spin sublevels. The exciton recombination in direct band gap semiconductors lasting at most up to a few nanoseconds occurs typically too fast to allow for ODMR detection. ODMR was observed, however, for negatively charged excitons (trions) in CdTe/(Cd,Mg)Te quantum wells where the long-living resident electrons interact with the microwave radiation [16]. Recently we demonstrated that the momentum separation of electrons and holes in heterostructures with an indirect band gap and a type-I band alignment, such as (In,Al)As/AlAs QDs, results in an increase of the exciton lifetime up to hundreds of microseconds [4,17,18], which allowed us to observe ODMR associated with long-living photoexcited electrons in

\*ivanov@ifpan.edu.pl

†tim@isp.nsc.ru

the  $X$  valley of the QDs [19]. The (In,Al)As/AlAs structures that were investigated in this study contained uncoupled QDs with strong exciton localization. In dense ensembles QDs can be coupled electronically, which results in spectral diffusion. Charge carrier redistribution among QDs can be assisted by microwave radiation, which has been scarcely studied so far for the indirect QDs.

In this paper we report on experimental studies of the exciton recombination and spin dynamics, as well as the effect of microwave radiation with 60 GHz frequency on the polarized exciton emission in a dense ensemble of (In,Al,Ga)As/(Al,Ga)As quantum dots. We demonstrate that: (i) The band alignment in these QDs is indirect of type I with the lowest electron states at the  $X$  minima of the conduction band and the top hole state at the  $\Gamma$  point of the valence band. (ii) Despite partly spectrally overlapping, the exciton emission from the QDs and the wetting layer can be distinguished by measuring their recombination dynamics, magnetic-field-induced circular polarization degree, and microwave-induced changes of the emission intensity and polarization. (iii) The charge carrier redistribution within the QD ensemble and wetting layer is decreased in strong magnetic fields. (iv) The  $g$  factor of 1.97 measured in ODMR has to be attributed to photoexcited electrons in the  $X$  valley.

## II. EXPERIMENTAL DETAILS

The studied self-assembled  $\text{In}_{0.4}(\text{Al}_{0.75}\text{Ga}_{0.25})_{0.6}\text{As}$  QDs, embedded in an  $\text{Al}_{0.75}\text{Ga}_{0.25}\text{As}$  matrix, were grown by molecular-beam epitaxy on a semi-insulating (001)-oriented GaAs substrate. The structure contains one layer of (In,Al,Ga)As QDs sandwiched between 50-nm-thick  $\text{Al}_{0.75}\text{Ga}_{0.25}\text{As}$  barriers, grown on top of a 250-nm-thick GaAs buffer layer. The top barrier was protected against oxidation with a 5-nm-thick GaAs cap layer. The QDs were formed at a temperature of 520°C. The nominal amount of  $\text{In}_{0.4}(\text{Al}_{0.75}\text{Ga}_{0.25})_{0.6}\text{As}$  deposited in the QD layer corresponds to about 9 monolayers (ML). The thickness of the wetting layer (WL) formed before the Stranski-Krastanov two-dimensional (2D) to three-dimensional (3D) transition, estimated by the reflection of high energy electron diffraction (RHEED) signal, is about 7 MLs. Therefore, the (In,Al,Ga)As QDs were formed on top of a relatively thick quantum well (compared to the typical corresponding values for InAs/GaAs QDs structures [20]). The density of the lens-shaped QDs is about  $(2-3) \times 10^{11} \text{ cm}^{-2}$ . The average dot diameter obtained by atomic force microscopy of uncapped dots is 20–25 nm [21]. The QD vertical size was estimated as 4–6 nm on the base of the RHEED picture change from 3D back to 2D during the QD overgrowth.

Let us take a closer look at the atomic and energy structures of the (In,Al,Ga)As/(Al,Ga)As heterostructure containing quantum dots and a wetting layer. The QDs formation takes place in Stranski-Krastanov growth mode. One can select the following stages during this process: (i) Layer-by-layer growth of a two-dimensional layer. This layer is strained due to a misfit of lattice parameters between the layer and the substrate materials. The associated strain energy increases rapidly with the increase of the wetting layer thickness. (ii) When the

critical thickness is reached the growth surface is rearranged to relieve the strain, which results in the QDs formation. (iii) The formed in such a way QDs (and wetting layer in the space between QDs) are covered with a matrix material during the overgrowth process. In our case, there are features in these QDs formation stages. In the first stage, the thickness of the wetting layer before it reaches the critical thickness is sufficiently high, and an inhomogeneous (in thickness) distribution of indium atoms takes place in this layer. The redistribution of the indium atoms occurs across the wetting layer as a result of the segregation process [22,23]. Thus, the upper part of the wetting layer with the critical thickness (in our case it is 7 MLs) is enriched with indium. In the second stage, the QDs are formed mainly from the material located on the surface of the wetting layer with critical thickness. Therefore, these QDs are enriched with indium, while the wetting layer under (and between) the QDs is depleted with indium. In the third stage, the formed QDs and the wetting layer in the space between the QDs are covered with a matrix material. The indium segregation also occurs during the overgrowth process. However, the faces of QDs are formed as planes with minimum surface energy [4]. These faces are very stable against segregation during the overgrowth, therefore, a sharp heterointerface is formed above the QD as shown in Ref. [4]. On the other hand, the overgrowth of the wetting layer in the space between QDs is accompanied by indium segregation. Since matrix material does not contain indium, the segregation here is even stronger than that at the initial growth stage before the QDs formation. The wetting layer around the QDs is additionally depleted in indium after overgrowth. Thus, the QDs lie on the wetting layer that has a band gap greater than that of QDs, and around the QDs inside the wetting layer there are small additional barriers.

Photoluminescence (PL) was excited by a semiconductor laser with a wavelength of 404 nm (photon energy of 3.07 eV). The excitation power density ( $P_{\text{ex}}$ ) was varied from  $10^{-6}$  up to  $1 \text{ W/cm}^2$ . The laser excitation spot on the sample has a diameter of 0.5 mm. In order to avoid optical orientation of carrier spins, we use linearly polarized laser light that excites photocarriers nonresonantly with large excess energy. The PL emission was dispersed by a 0.5-m monochromator, equipped with 300 grooves/mm diffraction grating. Typical spectral resolution was better than 2 meV. For the steady state measurements the PL was detected by a liquid-nitrogen-cooled charge-coupled-device (CCD) camera. For time-resolved measurements the photoluminescence was excited by a pulsed laser with a wavelength of 405 nm (3.07 eV) with a pulse duration of 50 ps. The detection was done by an avalanche silicon photodiode with a resolution in the time correlated single photon counting (TCSPC) mode of about 40 ps.

The PL spectra in external magnetic field were measured in different circular polarizations, from which the degree of circular polarization (DCP), defined as  $P_c(B) = (I^+ - I^-)/(I^+ + I^-)$ , was determined. Here  $I^+$  and  $I^-$  are the intensities of the  $\sigma^+$  and  $\sigma^-$  polarized PL components, respectively. The angle  $\theta$  between the magnetic field direction and the QD growth axis ( $z$  axis) was  $0^\circ$ , corresponding to the Faraday geometry. To determine the sign of  $P_c$ , we performed a control measurement on a diluted magnetic semiconductor

structure containing (Zn,Mn)Se/(Zn,Be)Se quantum wells for which  $P_c > 0$  in Faraday geometry [24].

For the ODMR experiments we used an all-solid state ultrastable microwave (MW) source operated in the range 59.25 to 60.75 GHz with a maximum power of 150 mW. The output MW power  $P_{MW}$  could be reduced by a variable attenuator down to 0.02 mW. The sample has in the plane dimensions 0.6 mm (width) and 4 mm (height). Thickness of the sample was 0.3 mm being mainly contributed by the substrate thickness. The sample was mounted in a cylindrical microwave cavity with the main mode  $TE_{011}$  along its main axis, and placed in the maximum of the H component of the electromagnetic field. Optical excitation of the sample and detection of its photoluminescence was achieved via four orthogonal apertures in the cavity walls. The cavity quality (Q factor) was varied in the range of 500–2500 in a regime of above-critical coupling. The cavity with the sample was placed in a split-coil magnet cryostat and exposed to a longitudinal magnetic field (Faraday geometry) up to  $B = 6$  T. For low temperature measurements it was immersed in pumped liquid helium ( $T = 1.9$  K).

The MW power was modulated synchronously with the CCD readout sequences by a *p-i-n* diode modulator with a dumping level of 50 dB. A scheme of the ODMR setup is given in Ref. [25]. The magnetic field dependencies of the MW-induced signals, i.e., the ODMR signals, are recorded by scanning the magnetic field. Measurements of PL in ODMR experiments have been provided at the same setup described above.

The MW induced PL dynamics measurements were done under steady state optical excitation and pulsed MW modulation. The PL kinetics was detected by an avalanche photodiode in multistop TCSPC mode synchronously with modulation of the MW power by a train of rectangular pulses with a duration of 10  $\mu$ s and on-off transition time of less than 5 ns. The MW power dumping level (MW off) exceeds 50 dB. The start of the TCSPC system was synchronized with the “on-off” transition of the MW pulse with a jitter of less than 1 ns.

### III. EXPERIMENTAL RESULTS

#### A. Energy level structure of QDs

In the studied structure the barrier material  $Al_{0.75}Ga_{0.25}As$  has an indirect band gap [26], i.e., the bottom of the conduction band is at the  $X$  point and the top of the valence band at the  $\Gamma$  point. The  $In_{0.4}(Al_{0.75}Ga_{0.25})_{0.6}As$  material composing the QDs has the band gap close to the direct-to-indirect ( $\Gamma$ - $X$ ) transition for bulk material, i.e., without accounting for the quantum confinement effects or strong strain in the pseudomorphic QDs. Thus, it is not *a priori* clear whether the wetting layer and the QDs formed in the  $In_{0.4}(Al_{0.75}Ga_{0.25})_{0.6}As/Al_{0.75}Ga_{0.25}As$  heterostructure have a direct or an indirect band gap and whether they show of type-I or type-II band alignment [27]. These possibilities are shown schematically in Fig. 1.

An experimental method for identifying the type of band alignment in low-dimensional heterostructures was proposed recently in Ref. [23]. It was shown that in a one monolayer

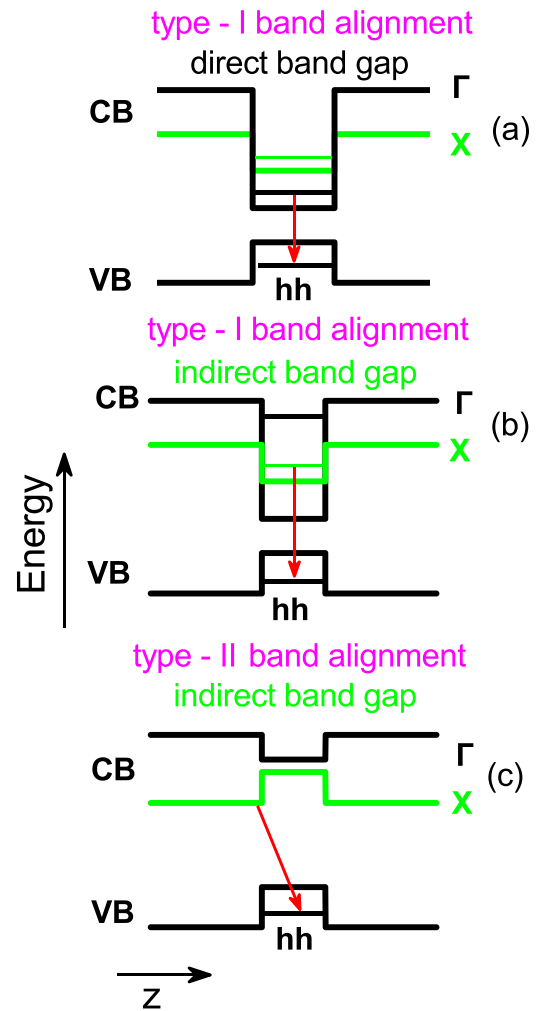


FIG. 1. Schematic energy structures that can be considered for the studied heterostructure: (a) Direct band gap with band alignment of type I, (b) indirect band gap with band alignment of type I, and (c) indirect band gap with band alignment of type II. Red arrows mark the different optical transitions related to the decay of the ground state exciton.

thick quantum well (QW) structure the PL maximum energy  $E_{max}$ , measured as a function of the excitation power density  $P_{ex}$ , is generally described by the following expression:

$$E_{max}(P_{ex}) - E_{max}(P_0) = a \ln\left(\frac{P_{ex}}{P_0}\right) + b\left(\frac{P_{ex}}{P_0}\right)^{1/3}. \quad (1)$$

Here  $a = U_e + U_h$ , where  $U_e$  and  $U_h$  are the parameters of the Urbach energy tails for electrons and holes, respectively,  $P_0$  is the minimum value of the used excitation power density, and  $b$  is a variable parameter. The logarithmic term describes the occupation of the electron states in QWs of both type-I and type-II band alignment. The second term takes into account the band bending, which appears with increasing concentration of electrons and holes in the type-II QWs due to their spatial separation, but is absent in type-I QWs where  $b \equiv 0$ . Note that in the dense ensemble of QDs (with dot density exceeding  $10^{11}$   $cm^{-2}$ ) carrier redistribution between the dots may occur, as we have shown for (In,Al)As/AlAs QDs [28,29]. Therefore, when we use Eq. (1) to determine the

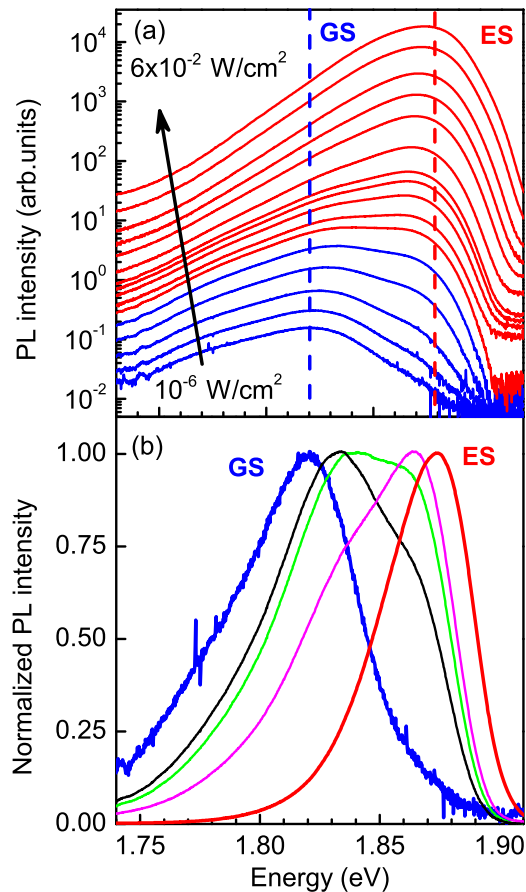


FIG. 2. (a) PL spectra of the studied QDs for various excitation power densities varied from  $10^{-6}$  up to  $6 \times 10^{-2}$  W/cm $^2$ .  $T = 1.9$  K. (b) Normalized PL spectra measured at  $P_{\text{ex}}$  from left to right:  $3 \times 10^{-6}$ ,  $6 \times 10^{-5}$ ,  $1 \times 10^{-4}$ ,  $3 \times 10^{-4}$ , and  $6 \times 10^{-2}$  W/cm $^2$ .

type of QDs the parameter  $a$  describes the occupation of the density of states (DOS) in an ensemble of coupled quantum dots.

PL spectra of the studied QDs measured at the low temperature of  $T = 1.9$  K at different excitation densities are shown in Fig. 2(a). Two lines can be identified in the broad PL band. The first line centered at lower energy of  $E_{\text{max}} = 1.82$  eV (GS line) dominates at low excitation densities. Its full width at half maximum (FWHM) is 65 meV at  $P_{\text{ex}} = 3 \times 10^{-6}$  W/cm $^2$ . With growing  $P_{\text{ex}}$  the intensity of the GS line tends to saturate, while a second line (ES) whose intensity increases fast with excitation power emerges on the high energy flank. Finally, the ES line dominates at high excitation densities, so that the GS transition can be recognized only as asymmetry of the emission band towards lower energies. The ES emission has a center energy of  $E_{\text{max}} = 1.874$  eV and a FWHM of 43 meV at  $P_{\text{ex}} = 6 \times 10^{-2}$  W/cm $^2$ . For better visualization of the transformation of the PL spectra we plot them normalized to their maximum intensity, using a linear scale, see Fig. 2(b).

Figure 3(a) shows the emission intensity of the GS and ES transitions as a function of the excitation power  $P_{\text{ex}}$ . The data for the two transitions are given only in the power ranges where the emission lines can be clearly separated. At low powers, before it saturates, the GS intensity rises linearly

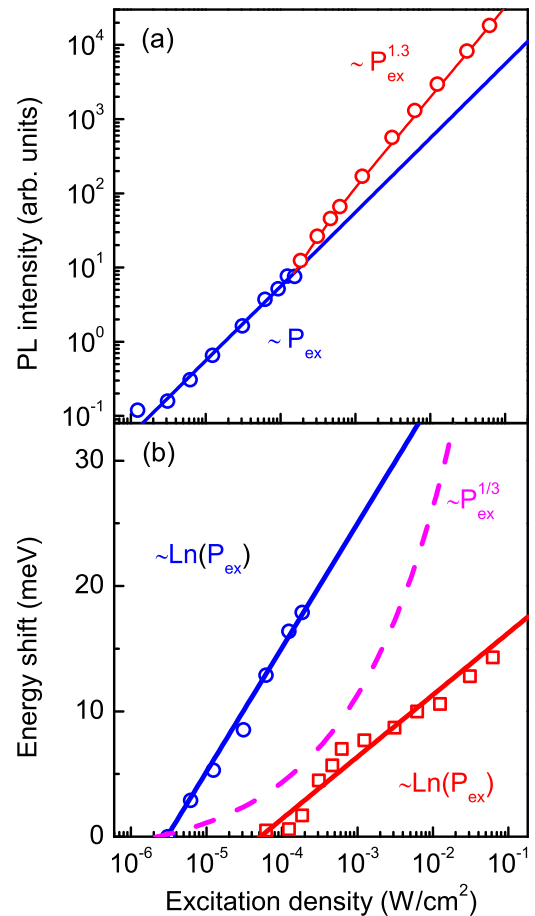


FIG. 3. (a) PL peak intensity of GS (blue circles) and ES (red circles) lines as a function of excitation density. Lines are interpolations of the data. (b) Shift of the PL maximum as a function of excitation density from their positions at the lowest excitation density. Color code is same as in (a). Solid lines are fits using Eq. (1) with parameters  $P_0 = 6 \times 10^{-6}$  W/cm $^2$ ,  $b = 0$ , and  $a = 4.3$  and 2.2 meV for the GS and ES lines, respectively. Dashed line shows the dependence for a QW structure with type-II band alignment with  $a = 0$  and  $b = 130$  meV.

with  $P_{\text{ex}}$ . At powers where the ES transition shows sufficient intensity, its power density dependence is slightly superlinear with an exponent of 1.3.

The GS and ES lines are attributed to the ground and excited states in the QDs, respectively. The lines are broad because of the dispersion in dot size, shape, and composition within the ensemble. Each QD in the ensemble has a ground and a first excited state. For dome-shaped QDs with approximately rotational symmetry about the growth axis, the GS can host only two electrons with opposite spin due to Pauli blocking. Additional carriers have to occupy the excited states. This state can host four electrons, the number of which is given by the (quasi-)degeneracy of states with orbital angular momentum component  $+1$  and  $-1$ , besides the two spin orientation possibilities.

This explains the higher emission intensity of the ES transition due to the twice larger density of states compared to the GS as shown schematically in Fig. 4. Furthermore, the dispersion of QD parameters is smaller for excited states due

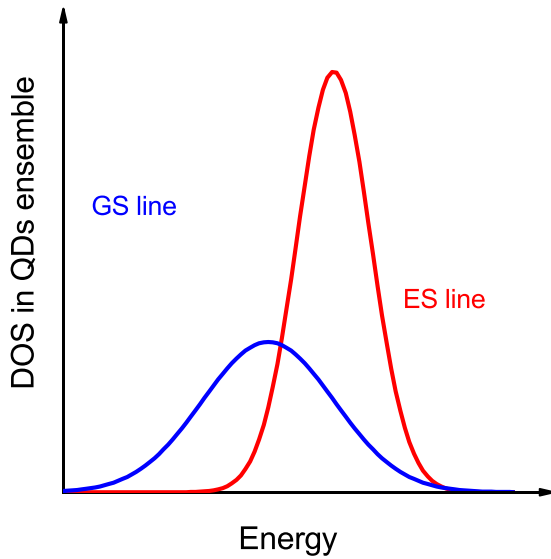


FIG. 4. Schematics for density of states in a QD ensemble. The blue contour corresponds to the ground state with twofold spin degeneracy and the red one to the first excited state, which is fourfold degenerate, assuming perfect rotational symmetry. Note that the integral of the ES contour is twice as large as that for the GS.

to the larger extension of their wave functions into the WL and barriers, reducing the sensitivity to the QD parameter dispersion. Indeed, we have shown in Ref. [30] that a narrowing of the ground electronic states distribution in (In,Al)As/AlAs QD ensembles takes place when decreasing the confinement barrier by high temperature annealing. This difference in DOS is a result of smaller FWHM.

The dependencies of the PL line shifts on the excitation power density are shown in Fig. 3(b). Both dependencies are well approximated by Eq. (1) with  $a = 4.3$  and  $2.2$  meV for the GS and ES lines, respectively. As it was expected parameter  $a$  is smaller for the ES line with narrower DOS distribution. For both lines  $b = 0$ , which allows us to conclude that the studied (In,Al,Ga)As/(Al,Ga)As QDs have a type-I band alignment. We show also in Fig. 3(b) by the dashed line the dependence expected for a QW with type-II band alignment.

To reveal the QD band structure (direct or indirect) in momentum space we measured the PL dynamics. The spectra recorded at different delays after the excitation pulse ( $t_d$ ) and integrated within a fixed time window ( $t_g$ ) are shown in Fig. 5. One can see that the ES line appears in the spectra right after the laser pulse and dominates during times up to several microseconds. The GS line appears with a delay of  $3 \mu\text{s}$  and becomes the strongest at subsequent PL decay times. Note that the faster disappearance of the excited state is typical for the PL dynamics in QDs.

The PL decays measured at various detection energies are shown in Fig. 6. The data are plotted using a double-logarithmic scale, which is convenient for presenting the dynamics across a wide range of decay times and PL intensities. In the spectral range of  $1.740\text{--}1.890$  eV the exciton recombination dynamics have two distinctive stages: (i) a fast decrease after the excitation pulse during  $70$  ns followed by

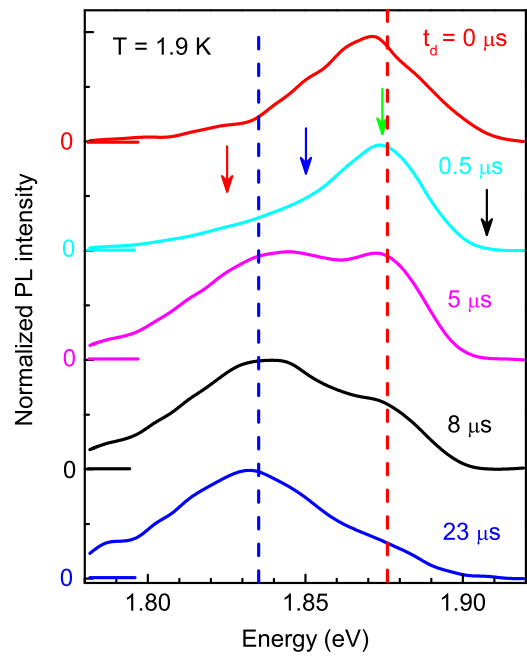


FIG. 5. Normalized PL spectra measured with different delays after the excitation pulse  $t_d$ , using different integration time windows  $t_g$  at  $T = 1.9$  K and excitation density of  $3.2 \times 10^{-3}$  W/cm<sup>2</sup>. From top to bottom  $t_d$  ( $t_g$ ) is equal to  $0 \mu\text{s}$  ( $20$  ns),  $0.5 \mu\text{s}$  ( $0.2 \mu\text{s}$ ),  $5 \mu\text{s}$  ( $2 \mu\text{s}$ ),  $8 \mu\text{s}$  ( $3 \mu\text{s}$ ), and  $23 \mu\text{s}$  ( $9 \mu\text{s}$ ). Dashed vertical lines mark the energies of the GS (blue) and ES (red) PL lines taken from the cw spectroscopy data. Arrows mark the energies of  $1.823$ ,  $1.850$ ,  $1.873$ , and  $1.906$  eV where the PL dynamics shown in Fig. 6 were measured.

(ii) a slower decay up to several tens of  $\mu\text{s}$ , which can be described by a power-law function. However, for energies above  $1.890$  eV the dynamics become faster. One can see that at the energy of  $1.906$  eV (black line) the signal disappears within  $0.1 \mu\text{s}$ .

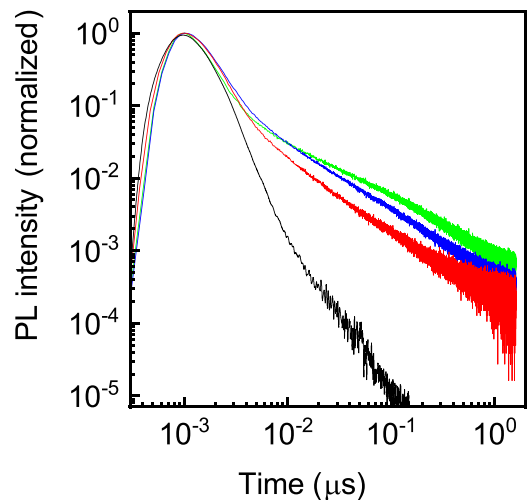


FIG. 6. PL dynamics measured at  $T = 1.9$  K at detection energies of  $1.823$  (red),  $1.850$  (blue),  $1.873$  (green), and  $1.906$  eV (black). PL excited by pulsed laser with a photon energy of  $3.07$  eV and a pulse duration of  $50$  ps. The time resolution for PL dynamics measurements was  $0.8$  ns.

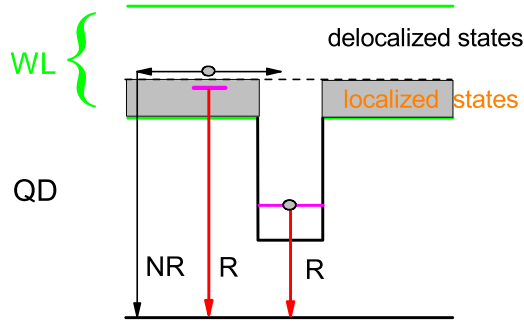


FIG. 7. Schematics for exciton dynamics in the QDs and wetting layer. Horizontal arrows indicate exciton motion along the wetting layer. Vertical arrows indicate nonradiative (NR) and radiative (R) recombination.

The observed PL dynamics are typical for indirect band gap QD and QW structures. The fast initial stage is a result of multiexciton recombination, as shown in Ref. [4]. The power-law PL dynamics is also inherent to ensembles of indirect band gap QDs, as we demonstrated for various materials systems: (In,Al)As/AIAs [4], (In,Al)(As,Sb)/AIAs [31], Ga(As,P)/GaP [32], and Ga(Sb,P)/GaP [33]. In this case the nonexponential exciton PL dynamics are caused by the contribution of excitons emitting at the same wavelength, but localized in QDs with different radiative recombination times (due to different sizes, shapes, and/or compositions) [4,34]. Thus, we conclude that in the studied (In,Al,Ga)As/(Al,Ga)As QDs the electrons involved in the optical transitions of both the GS and ES lines are localized in the  $X$  minimum of the QD conduction band.

It is interesting that the exciton states in the high-energy-tail of the PL spectrum (1.906 eV) differ from those in the spectral range of 1.740–1.890 eV. We will show below that the PL at 1.906 eV originates from exciton recombination in the wetting layer. The much faster recombination in the wetting layer may arise from faster radiative exciton recombination compared to QDs due to concentration of the wave function inside the light cone, as well as from exciton motion in the layer plane with subsequent capture into the QDs and/or nonradiative recombination centers. The latter is typical for Al-based heterostructures due to strong chemical reactivity for Al that results in defects formation [29,35]. These findings indicate a weak localization of the excitons due to the roughness of the wetting layer heterointerface, which we schematically illustrate in Fig. 7. This weak exciton localization is a result of the relatively large WL thickness of about 7 monolayers compared to about 1 monolayer thick WL in InAs/AIAs QDs [18].

### B. Photoluminescence in magnetic field

External magnetic fields applied in the Faraday geometry along the structure growth axis induce only small changes of the unpolarized PL. Its intensity slightly increases, as one can see in Fig. 8, and the recombination dynamics show no changes in fields up to 6 T (not shown).

In magnetic field the exciton spin levels are split by the Zeeman effect. The thermal population of these levels results in circular polarization of the exciton emission. This is

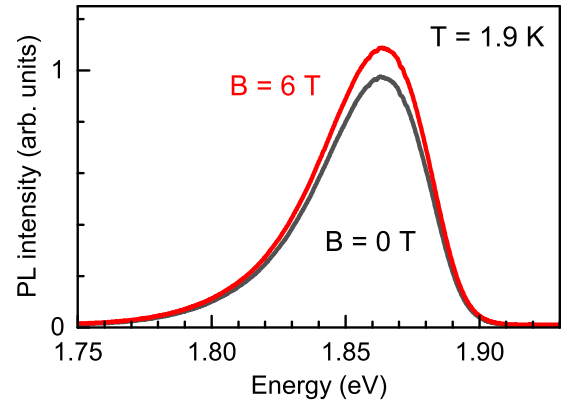


FIG. 8. Unpolarized PL spectra of the studied QDs measured at  $B = 0$  and 6 T for an excitation density of  $6 \times 10^{-2}$  W/cm<sup>2</sup>.

demonstrated in Fig. 9(a), where we show PL spectra measured for  $\sigma^+$  and  $\sigma^-$  circular polarization in a magnetic field of 6 T. The  $\sigma^+$  polarized component has a stronger intensity, which means that the magnetic-field-induced degree of circular polarization  $P_c$  is positive. Unexpectedly, the DCP has a significant spectral dependence. The polarization degree is about 0.19 at the low-energy side of the spectrum, while it is 0.35 at the high-energy side, as shown by the green line in Fig. 9(a). This evidences that the high energy side of the QDs emission band is contributed by states of different origin, namely the emission comes from the wetting layer. A possible reason of increase in polarization degree for the wetting layer is an increasing of bright exciton  $g$  factor in this layer comparing with the  $g$  factor in QDs. The MW induced changes in the optical spectra presented below give farther support for this interpretation. In both spectral regions the polarization degree increases monotonically with increasing the magnetic field strength, see Fig. 9(b).

The positive DCP in the studied, nominally undoped QDs allows us to exclude a possible contribution of negatively charged excitons (trions) to the QD emission. Indeed, the sign of negative trion DCP is determined by the sign of the heavy-hole  $g$  factor  $g_{hh}$ . We showed experimentally that  $g_{hh} > 0$  in (In,Al)As QDs, which results in a negative DCP for the trions [36].

The electron  $g$  factor  $g_e$  in the  $X$  valley is close to 2 and positive. Below we measure it by means of ODMR and get  $g_e = 1.97$ . The exciton  $g$  factor  $g_{ex}$  is made up of the electron and heavy-hole ones:  $g_{ex} = g_{hh} - g_e$  [37]. The measured  $P_c > 0$  corresponds to  $g_{ex} < 0$  [38–40]. Therefore, having a positive value,  $g_{hh}$  has to be smaller than  $g_e$ .

### C. Effect of microwave radiation and optically detected magnetic resonance

We turn now to the effects induced by MW radiation with a frequency of  $f_{MW} = 59.7$  GHz and a power of 100 mW. We start with its effect on the emission intensity, which does not exceed 1%, but nevertheless can be clearly detected. For that we plot in Fig. 10(a) the spectral dependence of the normalized difference of PL intensities measured with ( $I_{MW}$ ) and without ( $I_0$ ) MW radiation:  $(I_{MW} - I_0)/I_0$ . At zero magnetic field MW-induced changes are visible for the whole PL band

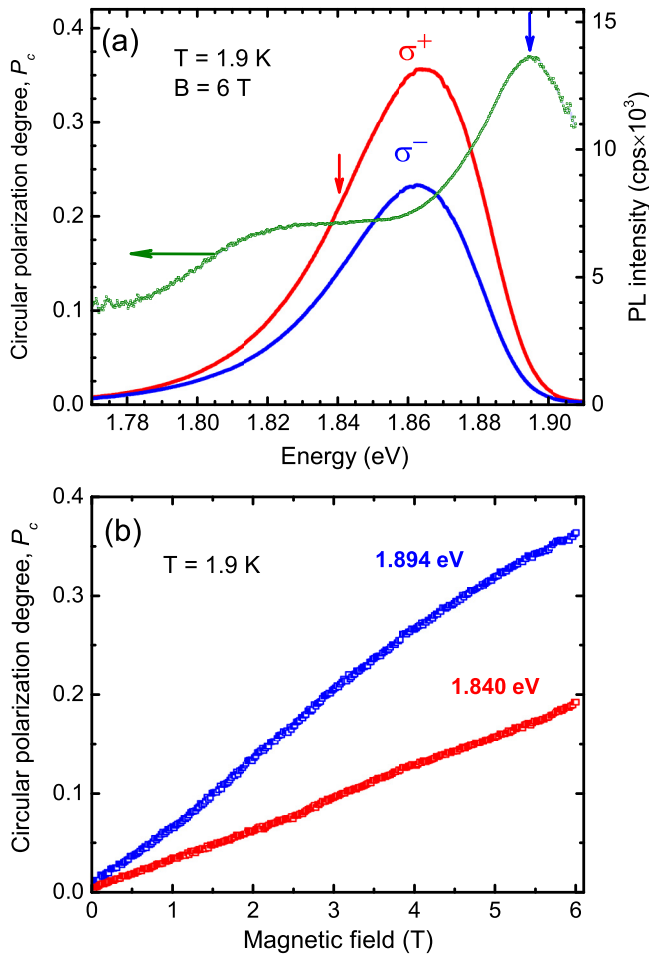


FIG. 9. Polarized PL in external magnetic fields measured at the excitation density of  $6 \times 10^{-2} \text{ W/cm}^2$ . (a)  $\sigma^+$  (red line) and  $\sigma^-$  (blue line) circularly polarized spectra at  $B = 6 \text{ T}$ . Green line shows the spectral dependence of the polarization degree. (b) Polarization degree at the energies of 1.894 (blue) and 1.840 eV (red), shown by the arrows in (a), as a function of magnetic field.

with a pronounced increase at the high energy side around 1.90 eV. The PL amplitude decreases under MW radiation, which we explain by an enhanced mobility of excitons and carriers heated by nonresonant MW absorption. The effect is stronger in the spectral range of the wetting layer from which excitons can be captured into the QDs or by nonradiative centers. In the dense QD ensemble the intensity decrease can be explained by enhanced transfer to QDs with nonradiative centers. This interpretation is confirmed by a strong decrease of the MW effect in a magnetic field of 6 T, see the red line in Fig. 10(a). It disappears for the QDs and is reduced by a factor of 2 for the WL. We explain this behavior by suppression of the exciton motion due to their enhanced localization caused by shrinking of the wave function and reduced tunneling [28,41–43]. The increase of the PL intensity in magnetic field of 6 T shown in Fig. 8 is in line with this explanation.

For the polarized emission in strong magnetic fields, e.g., at 4 T as shown in Fig. 10(c), the MW-induced changes coincide for the  $\sigma^+$  and  $\sigma^-$  circularly polarized spectra. From that we

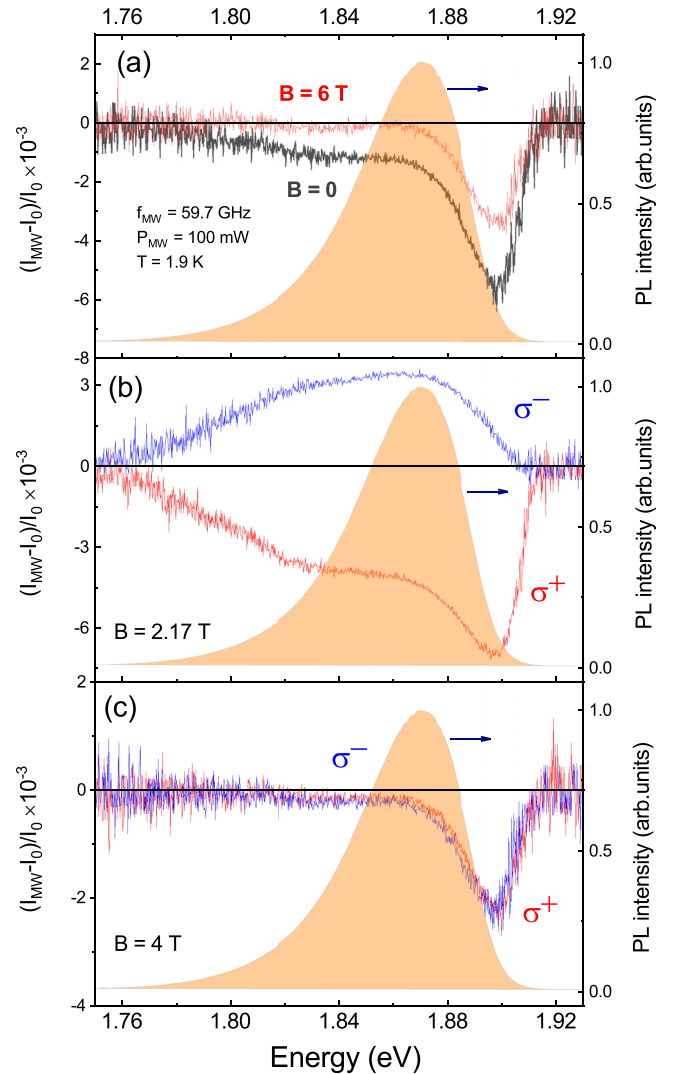


FIG. 10. Spectral dependence of the normalized variation of PL intensity under MW radiation with  $P_{MW} = 100 \text{ mW}$ . (a) Unpolarized signals measured at  $B = 0$  and 6 T. (b) Circularly polarized signals at  $B_R = 2.17 \text{ T}$ . (c) Circularly polarized signals at  $B = 4 \text{ T}$ . For convenience, the PL spectrum is shown in all panels by the orange area.

conclude that the effect at this field strength is dominated by variation of the integral PL intensity, and not of the emission polarization.

To have a comprehensive picture of the magnetic field dependence for the polarized emission and also search for spin resonances induced by the MW radiation, we present two-dimensional plots of the MW-induced changes in Fig. 11. Here the PL intensity is coded by colors (red for positive changes and blue for negative ones) as a function of the emission energy and the magnetic field varied from 0 up to 6 T. One clear resonance can be detected with the resonance field at  $B_R = 2.17 \text{ T}$ . In resonance, the  $\sigma^+$  polarized intensity decreases, while the  $\sigma^-$  one increases, evidencing the DCP decrease. The spectral dependence of these changes at  $B_R = 2.17 \text{ T}$  are shown in more detail in Fig. 10(b). Here, for the QD emission (see, e.g., 1.84 eV), the changes in both polarizations have very close absolute values. This means that the main

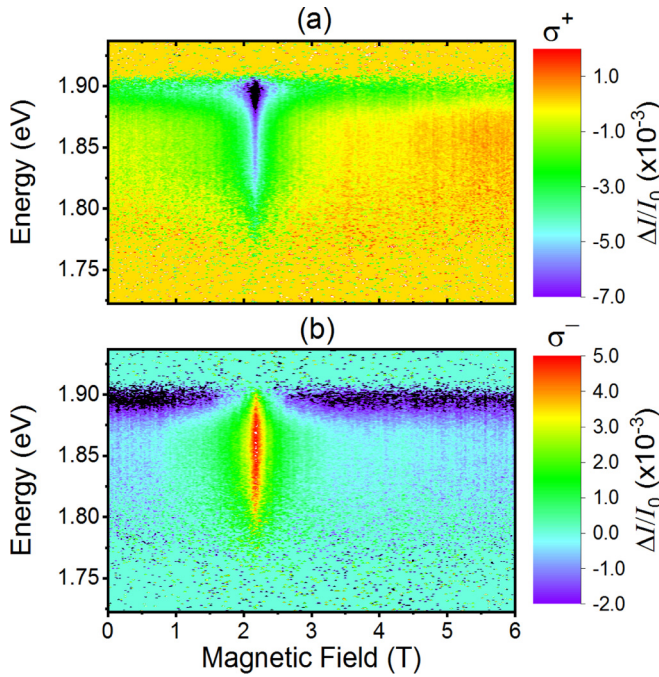


FIG. 11. Microwave induced variation of the  $\sigma^+$  (a) and  $\sigma^-$  (b) circularly polarized PL intensity as a function of the magnetic field. Each vertical line on the chart is a differential spectrum (PL spectrum modified under microwave radiation minus unperturbed PL spectrum) normalized on the unperturbed PL spectrum at a definite magnetic field. The magnetic field is increased with a step of 20 mT. Microwave radiation has a frequency  $f_{MW} = 59.7$  GHz and a power of 100 mW.  $T = 1.9$  K.

MW effect is a redistribution of the emission between the two polarizations and an effect on the integral intensity is nearly absent. On the other hand, for the WL emission at 1.90 eV, the changes are asymmetric, showing that both effects are contributed here.

The magnetic field dependence of the MW effect on the polarization, namely the variation of  $P_c$  under MW radiation measured at 1.84 eV, is shown in Fig. 12. The signal is zero at zero magnetic field, where  $P_c = 0$ , but also in strong magnetic fields exceeding 3.5 T. A very pronounced resonance with slightly asymmetric shape is present in between. It can be decomposed into three Lorentzians. Two of them are strong and have the same resonant field  $B_R = 2.17 \pm 0.02$  T, which corresponds to a  $g$  factor of  $1.97 \pm 0.02$ . Note that the same value was previously reported for electrons in the  $X$  valley of the (In,Al)As/AlAs QDs [19,39]. The narrow (broad) resonance has a full width at half maximum of 126 mT (670 mT). The resonance field and width of these two contributions do not change across the PL spectrum. It is interesting to note that in (In,Al)As/AlAs QDs, which also have an indirect band gap and a type-I band alignment, a much narrower ODMR resonance of the  $X$ -valley electron with a width of 17 mT was reported [19]. The strong broadening of the ODMR resonance in the studied (In,Al,Ga)As/AlAs QDs is most probably related to a stronger  $\Gamma$ - $X$  mixing, as these states have different  $g_e$ , but their energies are close to each other. The stronger mixing is also evidenced by the considerably faster recombination time of indirect excitons, compared to the dynamics

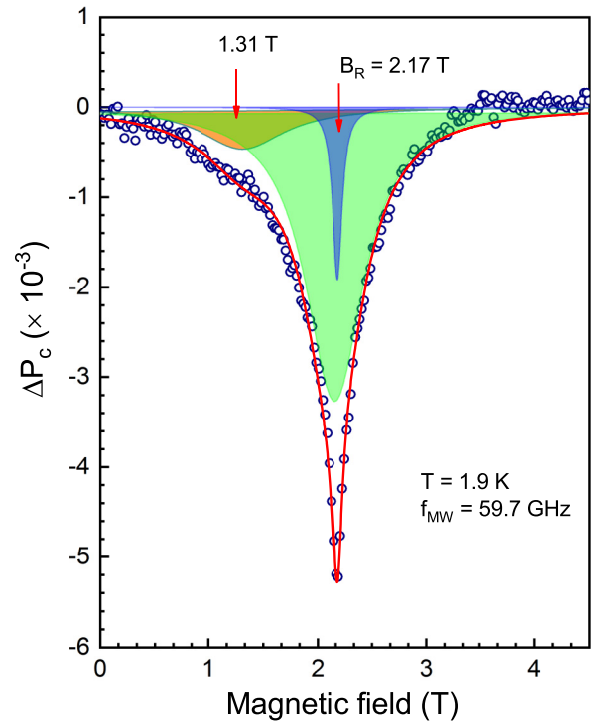


FIG. 12. ODMR signal in the circular polarization degree as a function of magnetic field at the detection energy of 1.84 eV. Experimental data is shown by open circles, spectrum components are indicated as color areas, cumulative fit is shown by the red line.

in (In,Al)As/AlAs QDs [19]. The presence of two resonances for the  $X$ -valley electrons can be attributed to electrons residing in the ground state (narrow resonance shown by blue area in Fig. 12) and excited states (broad resonance, green area) of the QDs or in the wetting layer.

We cannot identify the origin of the weak resonance with maximum at 1.31 T. It corresponds to a  $g$ -factor value of 3.26, which is too large for the values expected for the heavy

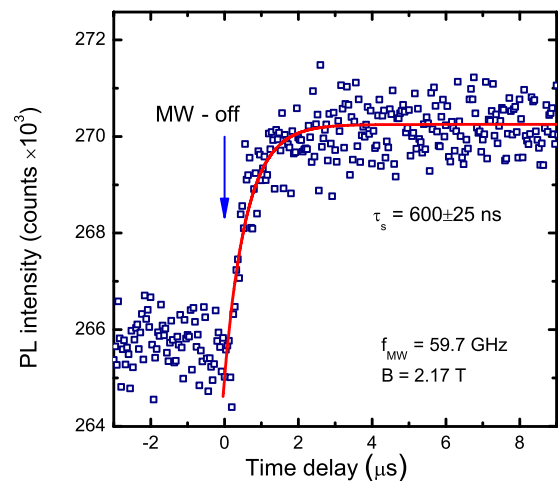


FIG. 13. Dynamics of the spin relaxation of the  $X$ -valley electrons measured via modulation of the MW intensity. The instrumental time resolution of 5 ns is limited by the rising and falling edges of the MW pulse.

hole and also for the electron in the  $\Gamma$  valley, as both should be smaller than  $g_e = 1.97$ . The signal can be tentatively related to cyclotron resonance of the electrons with an effective cyclotron mass  $m_c^* = 0.61m_0$  in the wetting layer or the barrier. This value of the cyclotron mass looks reasonable. The electron effective mass in the  $X$  valley of (Al,Ga,In)As alloy is not known. However, in binary alloys GaAs, InAs, and AlAs the electron effective mass in the  $X$  valley is varied in the range from  $0.2m_0$  up to  $1.0m_0$  depending on direction of the electron momentum [26].

The MW induced changes of the PL intensity allow us to measure the spin relaxation time of the  $X$ -valley electrons. For that we detect the time evolution of the PL intensity after switching off the MW radiation. The result is shown in Fig. 13, where the PL dynamics at  $B_R = 2.17$  T are presented. Fitting of these dynamics with a monoexponential function gives us  $\tau_s^e = 600 \pm 25$  ns. The variation of the spin relaxation time across the PL spectrum contour does not exceed level of experimental error of 10%. Such long times are characteristic for  $X$ -valley electrons in indirect QDs [7,10].

#### IV. CONCLUSIONS

The energy level structure, exciton recombination, and spin dynamics as well as ODMR have been studied for photoex-

cited electrons of (In,Al,Ga)As/(Al,Ga)As quantum dots. The QDs have an indirect, type-I band alignment with the lowest electron state of the QDs at the  $X$  minima of the conduction band. The exciton states in the QDs and wetting layer can be identified by measuring the time-resolved PL, magnetic field induced circular polarization degree and PL intensity while simultaneously applying microwave radiation. An ODMR resonance corresponding to a  $g$  factor of  $1.97 \pm 0.02$  has been identified, arising from the photoexcited electrons in the  $X$  valley. Our study shows that the ODMR technique is valuable for investigating QDs with indirect band gaps and long-living excitons, and can be developed for application to the large family of epitaxially and colloiddally grown QDs.

#### ACKNOWLEDGMENTS

This work was supported by the Deutsche Forschungsgemeinschaft via the Project No. 409810106 and by the Russian Foundation for Basic Research Grant No. 19-52-12001. T.S.Sh. acknowledges the financial support by the Russian Foundation for Basic Research (Grant No. 19-02-00098). V.Yu.I. acknowledges the support of the Polish National Science Center (Grant No. 2018/30/M/ST3/00276). M.B. acknowledges support by the Deutsche Forschungsgemeinschaft (ICRC TRR 160).

- 
- [1] Z. M. Wang, *Quantum Dot Devices* (Springer, New York, 2016).
- [2] Z. Yang, M. Gao, W. Wu, X. Yang, X. W. Sun, J. Zhang, H.-C. Wang, R.-S. Liu, C.-Y. Han, H. Yang, and W. Li, Recent advances in quantum dot-based light-emitting devices: Challenges and possible solutions, *Mater. Today* **24**, 69 (2019).
- [3] T. S. Shamirzaev, A. M. Gilinsky, A. K. Bakarov, A. I. Toropov, D. A. Tenne, K. S. Zhuravlev, C. von Borczyskowski, and D. R. T. Zahn, Millisecond photoluminescence kinetics in a system of direct-bandgap InAs quantum dots in an AlAs matrix, *Pisma Zh. Eksp. Teor. Fiz.* **77**, 459 (2003) [*JETP Lett.* **77**, 389 (2003)].
- [4] T. S. Shamirzaev, J. Debus, D. S. Abramkin, D. Dunker, D. R. Yakovlev, D. V. Dmitriev, A. K. Gutakovskii, L. S. Braginsky, K. S. Zhuravlev, and M. Bayer, Exciton recombination dynamics in an ensemble of (In,Al)As/AlAs quantum dots with indirect band-gap and type-I band alignment, *Phys. Rev. B* **84**, 155318 (2011).
- [5] T. S. Shamirzaev, J. Rautert, D. R. Yakovlev, J. Debus, A. Yu. Gornov, M. M. Glazov, E. L. Ivchenko, and M. Bayer, Spin dynamics and magnetic field induced polarization of excitons in ultrathin GaAs/AlAs quantum wells with indirect band gap and type-II band alignment, *Phys. Rev. B* **96**, 035302 (2017).
- [6] A. V. Khaetskii and Yu. V. Nazarov, Spin relaxation in semiconductor quantum dots, *Phys. Rev. B* **61**, 12639 (2000).
- [7] J. Rautert, T. S. Shamirzaev, S. V. Nekrasov, D. R. Yakovlev, P. Klenovsky, Yu. G. Kusrayev, and M. Bayer, Optical orientation and alignment of excitons in direct and indirect band gap (In,Al)As/AlAs quantum dots with type-I band alignment, *Phys. Rev. B* **99**, 195411 (2019).
- [8] O. Benson, C. Santori, M. Pelton, and Y. Yamamoto, Regulated and Entangled Photons from a Single Quantum Dot, *Phys. Rev. Lett.* **84**, 2513 (2000).
- [9] M. S. Kuznetsova, J. Rautert, K. V. Kavokin, D. S. Smirnov, D. R. Yakovlev, A. K. Bakarov, A. K. Gutakovskii, T. S. Shamirzaev, and M. Bayer, Electron-nuclei interaction in the  $X$  valley of (In,Al)As/AlAs quantum dots, *Phys. Rev. B* **101**, 075412 (2020).
- [10] D. S. Smirnov, T. S. Shamirzaev, D. R. Yakovlev, and M. Bayer, Dynamic Polarization of Electron Spins Interacting with Nuclei in Semiconductor Nanostructures, *Phys. Rev. Lett.* **125**, 156801 (2020).
- [11] B. C. Cavenett, Optically detected magnetic resonance (O. D. M. R.) investigations of recombination processes in semiconductors, *Adv. Phys.* **30**, 475 (1981).
- [12] P. G. Baranov and N. G. Romanov, Magnetic resonance in micro- and nanostructures, *Appl. Magn. Reson.* **21**, 165 (2001).
- [13] P. G. Baranov, H. J. von Bardeleben, F. Jelezko, and J. Wrachtrup, *Magnetic Resonance of Semiconductors and Their Nanostructures: Basic and Advanced Applications* (Springer, Wien, Austria, 2017).
- [14] V. Yu. Ivanov, M. Godlewski, D. R. Yakovlev, M. K. Kneip, M. Bayer, S. M. Ryabchenko, and A. Waag, Optically detected magnetic resonance in (Zn,Mn)Se/(Zn,Be)Se quantum wells, *Phys. Rev. B* **78**, 085322 (2008).
- [15] D. O. Tolmachev, V. Yu. Ivanov, D. R. Yakovlev, E. V. Shornikova, B. Witkowski, S. Shendre, F. Isik, S. Delikanli, H. V. Demir, and M. Bayer, Optically detected magnetic resonance in CdSe/CdMnS nanoplatelets, *Nanoscale* **12**, 21932 (2020).
- [16] C. Y. Hu, W. Ossau, D. R. Yakovlev, G. Landwehr, T. Wojtowicz, G. Karczewski, and J. Kossut, Optically detected magnetic resonance of excess electrons in type-I quantum wells with a low-density electron gas, *Phys. Rev. B* **58**, R1766 (1998).

- [17] T. S. Shamirzaev, A. V. Nenashev, and K. S. Zhuravlev, Coexistence of direct and indirect band structures in arrays of InAs/AlAs quantum dots, *Appl. Phys. Lett.* **92**, 213101 (2008).
- [18] T. S. Shamirzaev, A. V. Nenashev, A. K. Gutakovskii, A. K. Kalagin, K. S. Zhuravlev, M. Larsson, and P. O. Holtz, Atomic and energy structure of InAs/AlAs quantum dots, *Phys. Rev. B* **78**, 085323 (2008).
- [19] V. Yu. Ivanov, T. S. Shamirzaev, D. R. Yakovlev, A. K. Gutakovskii, Ł. Owczarczyk, and M. Bayer, Optically detected magnetic resonance of photoexcited electrons in (In, Al)As/AlAs quantum dots with indirect band gap and type-I band alignment, *Phys. Rev. B* **97**, 245306 (2018).
- [20] F. Patella, F. Arciprete, M. Fanfoni, A. Balzarotti, and E. Placidi, Apparent critical thickness versus temperature for InAs quantum dot growth on GaAs(001), *Appl. Phys. Lett.* **88**, 161903 (2006).
- [21] T. Ślupinski, K. P. Korona, J. Papierska, and J. Borysiuk, Efficient emission from InAlGaAs single quantum dots with low lattice misfit and AlGaAs indirect bandgap barrier, *Acta Phys. Pol. A* **130**, 1229 (2016).
- [22] P. Offermans, P. M. Koenraad, R. Notzel, J. H. Wolter, and K. Pierz, Formation of InAs wetting layers studied by cross-sectional scanning tunneling microscopy, *Appl. Phys. Lett.* **87**, 111903 (2005).
- [23] D. S. Abramkin, A. K. Gutakovskii, and T. S. Shamirzaev, Heterostructures with diffused interfaces: Luminescent technique for ascertainment of band alignment type, *J. Appl. Phys.* **123**, 115701 (2018).
- [24] D. Keller, D. R. Yakovlev, B. König, W. Ossau, Th. Gruber, A. Waag, L. W. Molenkamp, and A. V. Scherbakov, Heating of the magnetic ion system in (Zn,Mn)Se/(Zn,Be)Se semimagnetic quantum wells by means of photoexcitation, *Phys. Rev. B* **65**, 035313 (2001).
- [25] V. Yu. Ivanov, M. Godlewski, D. R. Yakovlev, S. M. Ryabchenko, G. Karczewski, and A. Waag, Time-resolved optically-detected magnetic resonance of II-VI diluted-magnetic-semiconductor heterostructures, *Phys. Status Solidi A* **204**, 174 (2007).
- [26] I. Vurgaftman, J. R. Meyer, and L. R. Ram-Mohan, Band parameters for III-V compound semiconductors and their alloys, *J. Appl. Phys.* **89**, 5815 (2001).
- [27] T. S. Shamirzaev, Type-I semiconductor heterostructures with an indirect gap conduction band, *Semiconductors* **45**, 96 (2011).
- [28] T. S. Shamirzaev, D. S. Abramkin, D. V. Dmitriev, and A. K. Gutakovskii, Nonradiative energy transfer between vertically coupled indirect and direct bandgap InAs quantum dots, *Appl. Phys. Lett.* **97**, 263102 (2010).
- [29] T. S. Shamirzaev, A. M. Gilinsky, A. K. Kalagin, A. I. Toropov, A. K. Gutakovskii, and K. S. Zhuravlev, Strong sensitivity of photoluminescence of InAs/AlAs quantum dots to defects: Evidence for lateral inter-dot transport, *Semicond. Sci. Technol.* **21**, 527 (2006).
- [30] T. S. Shamirzaev, A. K. Kalagin, A. I. Toropov, A. K. Gutakovskii, and K. S. Zhuravlev, Narrowing of ground energy level distribution in an array of InAs/AlAs QDs by post grown annealing, *Phys. Status Solidi (c)* **3**, 3932 (2006).
- [31] D. S. Abramkin, A. K. Bakarov, A. K. Gutakovskii, and T. S. Shamirzaev, Spinodal decomposition in InSb/AlAs heterostructures, *Semiconductors* **52**, 1392 (2018).
- [32] D. S. Abramkin, M. A. Putyato, S. A. Budennyi, A. K. Gutakovskii, B. R. Semyagin, V. V. Preobrazhenskii, O. F. Kolomys, V. V. Strelchuk, and T. S. Shamirzaev, Atomic structure and energy spectrum of Ga(As,P)/GaP heterostructures, *J. Appl. Phys.* **112**, 083713 (2012).
- [33] D. S. Abramkin, V. T. Shamirzaev, M. A. Putyato, A. K. Gutakovskii, and T. S. Shamirzaev, Coexistence of type-I and type-II band alignment in Ga(Sb,P)/GaP heterostructures with pseudomorphic self-assembled quantum dots, *JETP Lett.* **99**, 76 (2014).
- [34] J. Rautert, M. V. Rakhlin, K. G. Belyaev, T. S. Shamirzaev, A. K. Bakarov, A. A. Toropov, I. S. Mukhin, D. R. Yakovlev, and M. Bayer, Anisotropic exchange splitting of excitons affected by  $\Gamma$ -X mixing in (In,Al)As AlAs quantum dots, *Phys. Rev. B* **100**, 205303 (2019).
- [35] T. S. Shamirzaev, D. S. Abramkin, A. V. Nenashev, K. S. Zhuravlev, F. Trojanek, B. Dzurnak, and P. Maly, Carrier dynamics in InAs/AlAs quantum dots: Lack in carrier transfer from wetting layer to quantum dots, *Nanotechnology* **21**, 155703 (2010).
- [36] D. Dunker, T. S. Shamirzaev, J. Debus, D. R. Yakovlev, K. S. Zhuravlev, and M. Bayer, Spin relaxation of negatively charged excitons in (In,Al)As/AlAs quantum dots with indirect band gap and type-I band alignment, *Appl. Phys. Lett.* **101**, 142108 (2012).
- [37] A. A. Sirenko, T. Ruf, M. Cardona, D. R. Yakovlev, W. Ossau, A. Waag, and G. Landwehr, Electron and hole  $g$ -factors measured by spin-flip Raman scattering in CdTe/(Cd,Mg)Te quantum wells, *Phys. Rev. B* **56**, 2114 (1997).
- [38] T. S. Shamirzaev, J. Debus, D. R. Yakovlev, M. M. Glazov, E. L. Ivchenko, and M. Bayer, Dynamics of exciton recombination in strong magnetic fields in ultrathin GaAs/AlAs quantum wells with indirect band gap and type-II band alignment, *Phys. Rev. B* **94**, 045411 (2016).
- [39] J. Debus, T. S. Shamirzaev, D. Dunker, V. F. Sapega, E. L. Ivchenko, D. R. Yakovlev, A. I. Toropov, and M. Bayer, Spin-flip Raman scattering of the  $\Gamma$ -X mixed exciton in indirect band gap (In,Al)As/AlAs quantum dots, *Phys. Rev. B* **90**, 125431 (2014).
- [40] T. S. Shamirzaev, J. Rautert, D. R. Yakovlev, M. M. Glazov, and M. Bayer, Intrinsic and magnetic-field-induced linear polarization of excitons in ultrathin indirect-gap type-II GaAs/AlAs quantum wells, *Phys. Rev. B* **99**, 155301 (2019).
- [41] A. O. Govorov, Spin and energy transfer in nanocrystals without tunneling, *Phys. Rev. B* **68**, 075315 (2003).
- [42] V. F. Sapega, M. Cardona, and K. Ploog, Spin-flip Raman scattering in GaAs/AlGaAs multiple quantum wells, *Phys. Rev. B* **45**, 4320 (1992).
- [43] J. E. Zucker, E. Isaacs, D. Heiman, A. Pinczuk, and D. S. Chemla, Localized quantum well excitons in the high magnetic field limit, *Surf. Sci.* **196**, 563 (1988).